

A simple 2-D explanation for negative phases in TE magnetotelluric data

K. Selway,¹ S. Thiel¹ and K. Key²

¹Centre for Tectonics, Resources and Exploration, School of Earth and Environmental Sciences, University of Adelaide, South Australia 5005, Australia.
E-mail: katherine.selway@adelaide.edu.au

²Scripps Institution of Oceanography, University of California San Diego, 9500 Gilman Drive, La Jolla, CA 92093-0225, USA

Accepted 2011 November 20. Received 2011 November 20; in original form 2010 November 25

SUMMARY

We present magnetotelluric (MT) data collected in central Australia that display unusual negative transverse electric (TE) phases. Previous explanations for anomalous TE phases on land have relied on anisotropy, complicated 3-D geometries or coherent noise. In contrast, the central Australian data are free from coherent noise while phase tensor analysis shows that the survey region is 2-D and that the negative phases are an inductive effect. The survey was carried out in a grid that covers resistive basement rocks and conductive sedimentary cover. Stations located on the resistive basement display normal phase behaviour while stations located on the conductive cover display negative TE phases at periods of 0.01–0.1 s. Forward modelling of the region and inversion of the data shows that a shallow, laterally extensive, bounded conductor that overlies a resistor can produce the observed negative TE phases. An investigation of TE Poynting vectors for such a system shows that there is a ‘collision zone’ near the bounding edge of the conductor where energy that is diffusing downwards collides with energy that has been inductively coupled to the conductor and is diffusing upwards. At the base of the conductor this causes a cusp in TE apparent resistivity and phases that wrap through 360°, a phenomenon previously observed in the ocean-side of the TE coast effect. Negative phases extend to the surface of the conductor, where measurements are made in a land MT setting. The resistivity contrast between the conductive and resistive zones must be at least 1000 to produce negative phases for land MT. The period range and distance from the boundary of the conductor at which the negative phases are observed can be estimated from a combination of the thickness of the conductor and the resistivities of the two zones. The results presented here are the first example of an isotropic 2-D setting producing negative phases on land and represent an alternative explanation for observations of anomalous data.

Key words: Electrical properties; Electromagnetic theory; Magnetotelluric; Marine electromagnetics; Australia.

1 INTRODUCTION

The magnetotelluric phase (φ) is the argument of the complex magnetotelluric (MT) impedance. In geoelectrically 1-D settings, in which the resistivity of the earth changes only with depth, the MT phase will always lie in the range $0^\circ < \varphi < 90^\circ$ (Weidelt 1972). The same has generally been thought to be true for isotropic 2-D settings, in which the resistivity of the earth changes with depth and in one lateral direction. In 2-D settings, the MT impedance tensor decomposes into two independent modes, the transverse electric (TE) mode where the electric field is measured parallel to geoelectric strike while the magnetic field is perpendicular, and the transverse magnetic (TM) mode where the electric field is measured perpendicular to strike while the magnetic field is parallel. Weidelt & Kaikkonen (1994) showed that 2-D TM mode responses share the same phase constraints as 1-D responses, and therefore

the TM phases must lie in the range $0^\circ < \varphi < 90^\circ$. The only documented isotropic 2-D scenario in which phases lie outside of the $0^\circ < \varphi < 90^\circ$ range is the ocean-side of the TE mode coast effect, which can produce out of quadrant TE phases (both less than 0° and greater than 90°). These are interpreted to be caused by large, induced electrical currents that flow along the edge of the conductive ocean and the associated anomalous TE magnetic fields which wrap around the electric currents, eventually tipping past vertical, reversing the horizontal magnetic field and producing the anomalous phase (e.g. Fischer *et al.* 1978; Fischer 1979; Ferguson 1988; White & Heinson 1994; Schwalenberg & Edwards 2004; Constable *et al.* 2009; Key & Constable 2011). Modelling to understand this effect was first described in Fischer *et al.* (1978) and Fischer (1979), showing that for a structure consisting of a half-space of moderate resistivity with a mathematically thin, perfect conductor extending over half the surface, the TE magnetic field wraps around the edge of the

conductive sheet, reversing in direction beneath the sheet (Fischer 1979). More detailed finite element modelling was carried out by Constable *et al.* (2009), who included realistic sea depths, seafloor resistivities and bathymetry data from the San Diego Trough. The forward models show that electric field flow lines steepen near the centre of the trough, producing TE apparent resistivity cusps and anomalous phases. The effect has been further investigated by Key & Constable (2011) in response to data from offshore northeastern Japan that exhibit TE apparent resistivity cusps and phases that reach values as negative as -65° . Transfer functions calculated between marine stations and a land-based remote station show that the anomalous TE behaviour is an inductive distortion that is largely confined to the magnetic field. Poynting vector analysis shows that the TE energy flux curves upwards at depth and diffuses back to the seafloor due to strong inductive coupling between the conductive ocean and the resistive seafloor. The authors devised empirical equations that are consistent with their observations that both the period and the distance from the coastline at which the TE negative phases and apparent resistivity cusps appear increase with the seafloor resistivity and ocean depth.

Physically, the structure required to produce the negative phases observed in the ocean side of the coast effect is a relatively thin, high conductivity region that has at least one bounding edge and is in contact with a surrounding region of considerably greater resistivity. A coastal environment, where the ocean is the conductor, the thinly sedimented crust beneath the ocean and along its landward side is the resistor and the coastline is the conductor's bounding edge, is an obvious example of such a setting. However, there is no *a priori* reason why such features should only be observed in a coastal environment. If the necessary physical components exist on land it would be expected that the same features should be observed in land-based MT measurements. Parker (2010) produced a theoretical formulation for such a scenario in an investigation of whether 2-D TE responses can be matched by a 1-D response, inspired by the pioneering 2-D TM mode study of Weidelt & Kaikkonen (1994). Analysis showed that a thin sheet of high conductivity that is bound on each side and below by a perfect resistor has a TE response that cannot be approximated by a 1D model at any frequency and also produces negative phases at short periods (Parker 2010). This theoretical investigation provides an example of a general system that will produce negative phases, whether that system is on land or in the marine environment.

We present broad-band MT data from central Australia that were collected in a setting that is comparable to that described by Parker (2010), in which shallow, low resistivity sedimentary cover is bound on one margin and below by highly resistive basement rocks. The TE mode responses from the data set behave in the manner predicted by Parker (2010) and are also analogous to marine data sets, with negative phases at short periods observed from stations on the low resistivity zone. In land settings, anomalous phases have historically been attributed to inductive effects involving complex 3-D geometries or anisotropy that lead to current reversals (Heise & Pous 2003; Weckmann *et al.* 2003a,b; Ichihara & Mogi 2009; Thiel *et al.* 2009) or more recently were attributed to galvanic distortion (e.g. Lilley & Weaver 2010). In some cases, the anomalous phases have been conclusively shown to be due to local coherent noise (e.g. Egbert 1997; Egbert 2002). Egbert (1997) notes that in the presence of strong coherent noise the imaginary parts of the impedance tensor are small but reversed, resulting in the 'physically unreasonable negative phase'. In contrast, the data presented here, combined with the theoretical foundation of Parker (2010), show that there are simple, 2-D settings in which negative phases are both

reasonable and predictable. We explore the range of physical conditions necessary to produce negative TE mode phases and show that they are produced by the same processes as those observed for the ocean side of the TE coast effect.

2 MT SURVEY AND DATA

MT data were collected in central Australia in 2010 March in a 2×2.5 km grid consisting of 28 stations with spacing between 250 and 500 m (Fig. 1) with the aim of imaging the near-surface expression of the Cambrian Woodroffe Thrust (Camacho *et al.* 1995). Data were collected in a grid that was oriented as close as practicable to north-south. North-south 'columns' of the grid are named with the first four digits of the easting on which they are centred while east-west 'rows' are named from A in the south to F in the north (Fig. 1). Four-component data were collected, comprising two horizontal orthogonal magnetic fields measured with induction coil magnetometers and two horizontal orthogonal electric fields measured using copper/copper sulphate porous pots as electrodes in an L-shaped array, with field measurements aligned with magnetic north and east. Data were recorded at a sampling rate of 500 Hz for approximately 24 hr at each station.

At the southern end of the survey grid, stations were deployed in small patches of dirt around outcropping basement rock. The basement consists of high-grade metamorphic rocks of the northern Musgrave Province including mylonites, ultramylonites and pseudo-tachylytes of the Woodroffe Thrust (Camacho *et al.* 1995; Wade *et al.* 2008). Previous long-period MT surveys have shown the Musgrave Province basement to be highly resistive (Selway *et al.* 2009; Selway *et al.* 2011), potentially due to its high-grade, anhydrous nature. Shallow holes of approximately 15 cm depth were dug to bury the magnetometers and electrodes; subcropping rock was consistently encountered while digging, showing that basement rocks were very close to the surface. Subcropping rocks were observed in dry creekbeds aligned with stations in the east-west row B (Fig. 1), showing that the cover thickness at these locations is less than 1 m. The sedimentary cover thickens with distance north across the survey grid. Subcropping rocks were not observed in any more northerly creekbeds and the thickness of cover in the north of the survey grid is unknown. The sedimentary cover consists of Quaternary transported sand, talus and scree (Edgoose *et al.* 1993). Such sedimentary cover in Australia often has very low resistivities (e.g. Asten 1992; Macnae *et al.* 2001). Vegetation becomes significantly more dense to the north near row D (Fig. 1), suggesting a significant change in the depth or nature of the regolith at this point.

Data were processed using a bounded-influence remote-reference MT response method (Chave & Thomson 2004) to produce estimates of the impedance, apparent resistivity and phase. Apparent resistivity and phase data for several stations are shown in Fig. 2. Stations from a given row (B, C or D) for the columns 2150, 2160 and 2165 of the grid are plotted together since the responses from stations on the same row show consistent apparent resistivity and phase behaviour. Phase tensor analysis (Caldwell *et al.* 2004) was carried out on all stations and phase tensor ellipses at periods 0.01 s and 25 s are shown in Fig. 3. Strike directions determined from phase tensor analysis at periods less than approximately 1 s are consistently about 90° (Fig. 3). At periods longer than approximately 1 s, the phase tensor ellipse orientation becomes approximately north-south for all stations, with generally low skew values (Fig. 3). The behaviour of the stations is consistent along each east-west row but changes along each north-south column, suggesting an

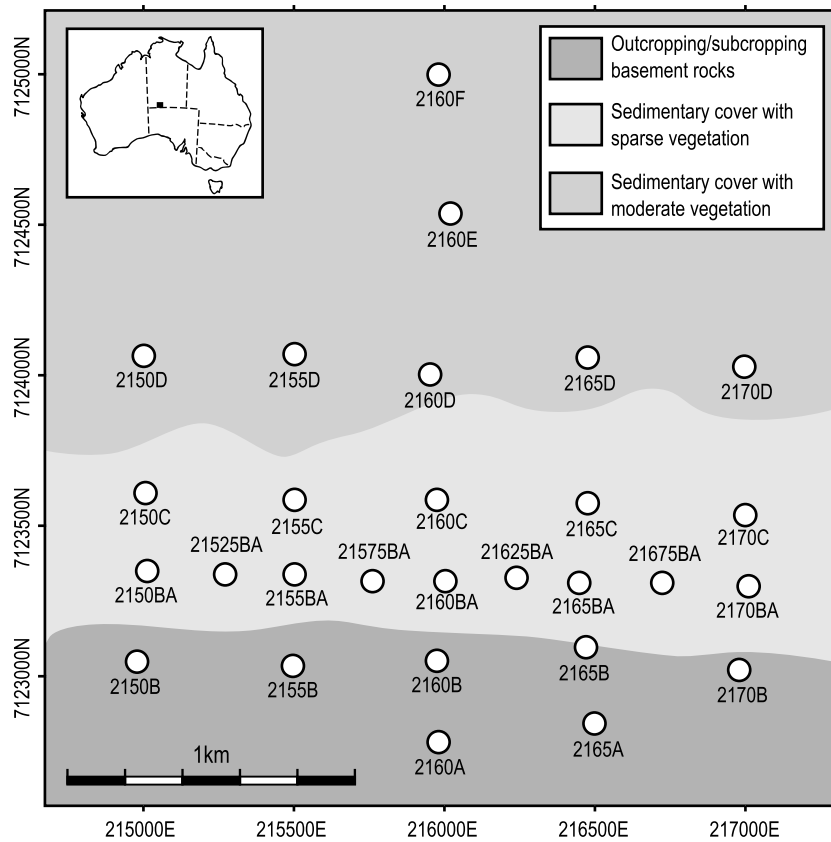


Figure 1. Map showing the locations of MT stations (circles) with relation to the mapped extent of subcropping basement rocks and a change from sparse to denser vegetation which is interpreted to indicate a change in the depth or type of sedimentary cover.

east–west strike direction. Regional geological data support an approximately east–west strike since major structures in the region all display roughly east–west trends (e.g. Camacho *et al.* 1995; Wade *et al.* 2008) and the mapped strike of cover–basement contacts are also approximately east–west (Fig. 1). Although the phase tensors exhibit a north–south elongation at longer periods, we suggest that the data are still responding to an approximately east–west strike, with regional structures juxtaposing a more resistive region containing the survey area with a more conductive region that sits to either the south or the north, since there are no known northerly striking features in the region. The Woodroffe Thrust, which outcrops in the south of the survey area and dips shallowly to the south, could be the causative structure if it juxtaposes a lower resistivity hanging wall with a higher resistivity footwall. Phase tensor skew values reaching approximately 7° are observed at most stations at periods of approximately 1 s and these higher skew values are likely to be due to the change in orientation of the current flow from shallow to regional features. We therefore define the mode comprising the east–west electric field and the north–south magnetic field to be the TE mode and that comprising the east–west magnetic field and the north–south electric field to be the TM mode.

Similar phase values between adjacent stations but vertical shifts in apparent resistivity curves suggest that static shifting is affecting both the TE and TM modes. At the southern end of the survey area (represented by stations in rows B and C), where subcropping rocks are close to the surface, apparent resistivity and phase data have normal MT characteristics with phases in the range $0^\circ < \varphi < 90^\circ$. However, most stations in row D and all stations to the north show TE mode phases that are negative at the short periods of 0.01–0.1 s. For

many stations, the negative phases become larger with decreasing period to an average maximum of approximately -5° at 0.008 s. The largest negative phase calculated is -11° at a period of 0.008 s at station 2160E. One common explanation for negative phases on land is coherent noise (e.g. Egbert 1997). Coherent noise is unexpected at this location due to its remoteness, approximately 100 km from any settlement. It is also unlikely that coherent noise would affect only the TE mode and not the TM mode. Moreover, the distinct spatial pattern of the responses, with stations in the north of the survey demonstrating the negative TE mode phase behaviour but stations in the south not displaying this behaviour, suggests that this behaviour is due to a phenomenon associated with the subsurface structure. Finally, data at stations that display negative TE mode phases were collected at the same time as data at stations that do not display this behaviour. If coherent noise were the cause of the negative phases, it would have affected all stations being recorded at the time the noise was present. Therefore we are confident that the observed negative phases in the TE mode are not caused by coherent noise.

3 PHASE TENSORS AND DISTORTION ANALYSIS

The distortions observed in MT data can be categorized as either inductive or galvanic (Jiracek 1990). Inductive distortions are related to the attenuation and phase shift of the induced fields, resulting in both amplitude and phase distortions. Conversely, galvanic distortions are related to charge build-up on lateral conductivity

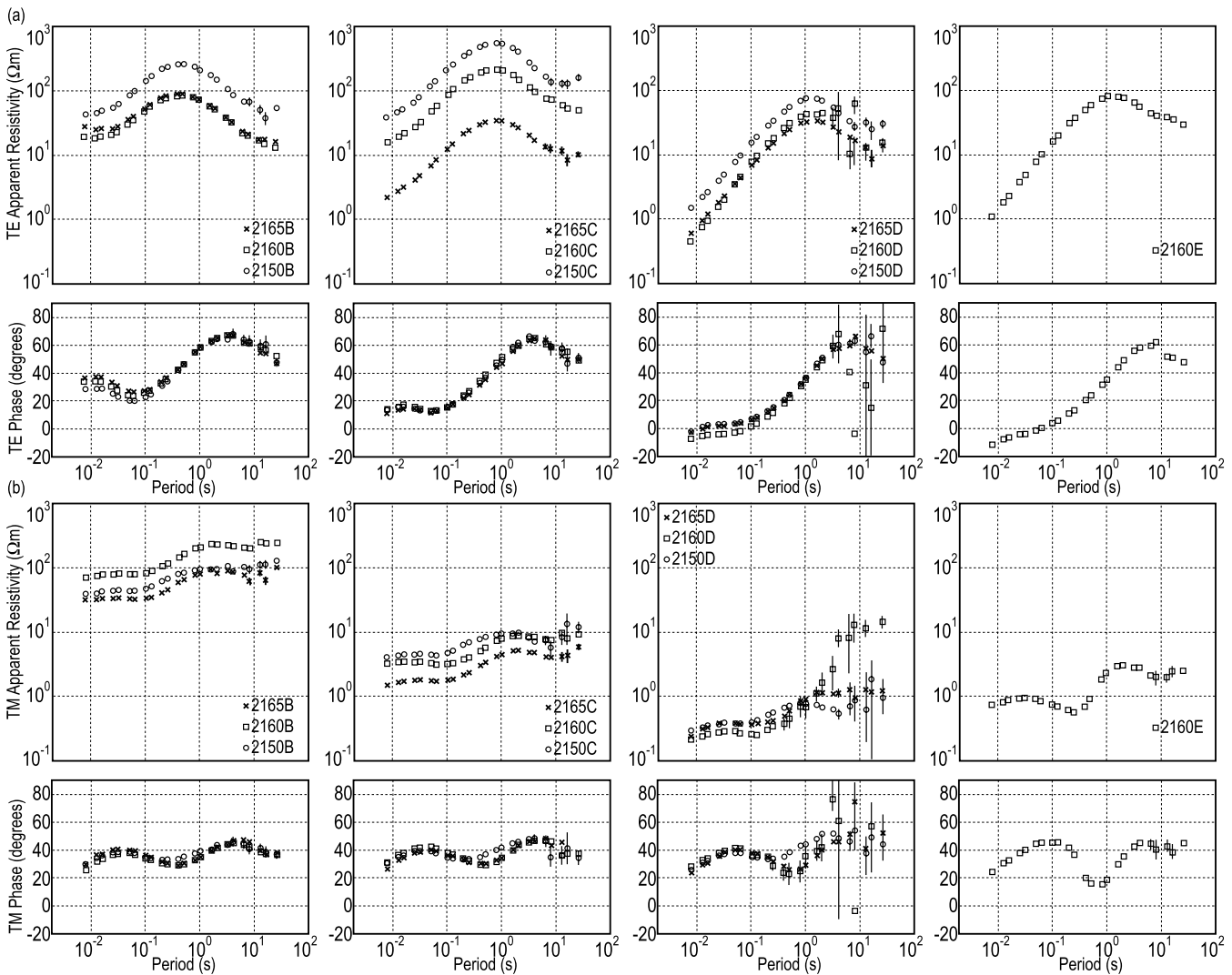


Figure 2. Responses from stations on rows B, C, D and E and columns 2150 (circles), 2160 (squares) and 2165 (crosses) for the TE mode (a) and the TM mode (b). Responses show consistency at stations across east–west rows, with most differences seemingly attributable to static shifts in the apparent resistivity. Responses from rows B and C, both in the southern half of the survey area, are similar whereas responses from rows D and E show very different behaviour including negative phases in the TE mode at short periods.

boundaries that result in only an amplitude shift in the electric field near the boundary. In the pure 2-D case, inductive distortions can be present in both TE and TM modes, whereas galvanic effects can only be present in the TM mode. When the distorting structure is a small-scale 3-D feature imbedded in a regional 2-D background, both TE and TM modes can have galvanic distortions. Because galvanic effects do not affect the phase, we expect that that our negative phases are due to inductive effects. However, to further demonstrate this point we considered a recent innovation for mitigating galvanic distortion through the use of the magnetotelluric phase tensor, which is immune to purely galvanic distortions (Caldwell *et al.* 2004). A key benefit of the phase tensor analysis is the ability to determine the geoelectric dimensionality and regional strike. Phase tensors for stations in rows D, E and F at periods shorter than approximately 1 s demonstrate extremely high ellipticities with strike direction at approximately 90° (Fig. 3). These are data for which the TE phase is approaching negative values. Phase tensors from data exhibiting negative phases are not plotted as the results may not be mean-

ingful. High ellipticities for data points exhibiting such behaviour were also observed in the phase tensor analysis of marine data by Key & Constable (2011). Phase tensors for more southerly stations have significantly lower ellipticities and low skew values with strike values remaining at approximately 90°.

Although galvanic distortions only affect the amplitude of the impedance and therefore are not expected to produce the observed negative phases, for completeness we applied phase tensor decomposition (Bibby *et al.* 2005) to examine if any galvanic effects are also present in the data. The estimation of the distortion tensor (*D*) to within a constant is possible if a 1-D section in the impedance response exists, a condition that is met in the station data between periods of approximately 0.01 and 0.05 s. In this case, the constraint on *D* is $\det(D) = 1$ (Bibby & Hohmann 1993; Bibby *et al.* 2005). A typical result of distortion removal from a northerly station (station 2160E) is shown in Fig. 4. As expected, distortion removal has not affected the negative phase values. In fact, for periods at which the TE phase is negative, the phase tensor invariant minimum

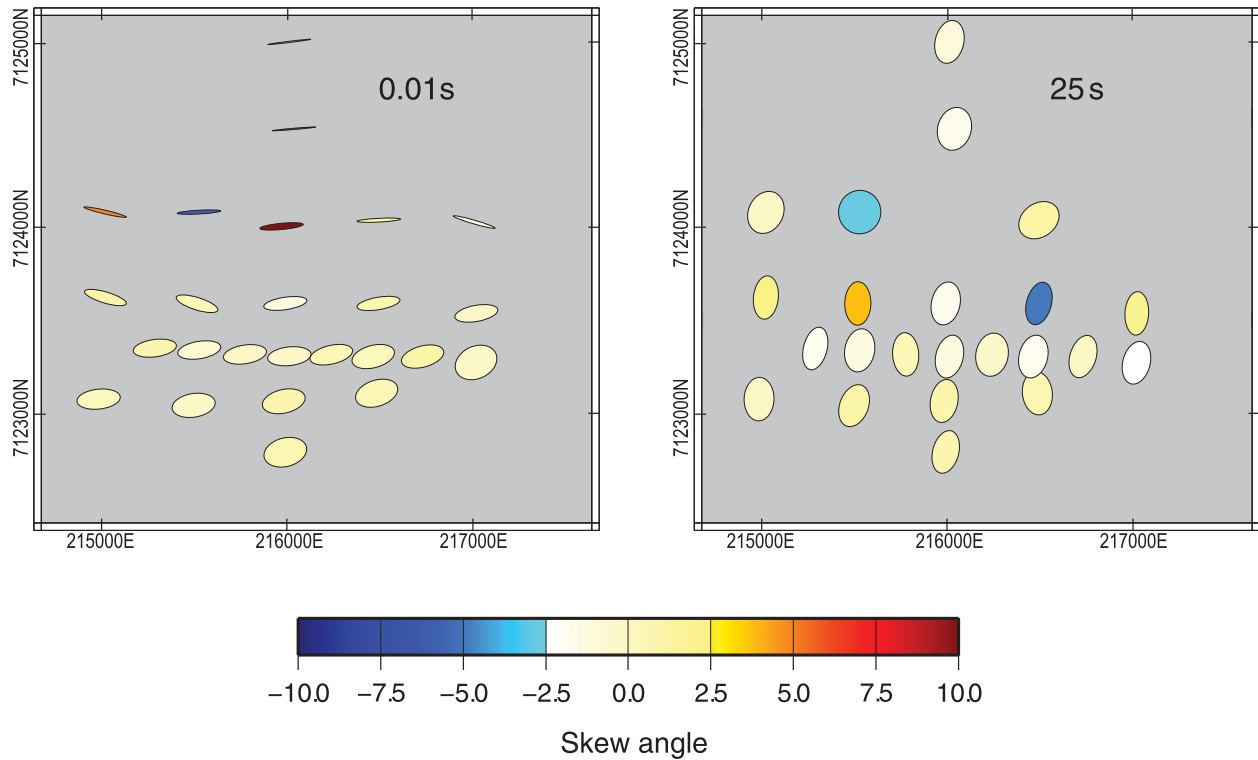


Figure 3. Phase tensor ellipses at periods 0.01s and 25 s, shaded for the skew of the tensor. At 0.01 s, the tensors are oriented approximately east–west and tensors from all stations in rows D, E and F (refer Fig. 1) are highly elliptical. At 25 s, all ellipses are oriented approximately north–south with moderate ellipticities and low skew values.

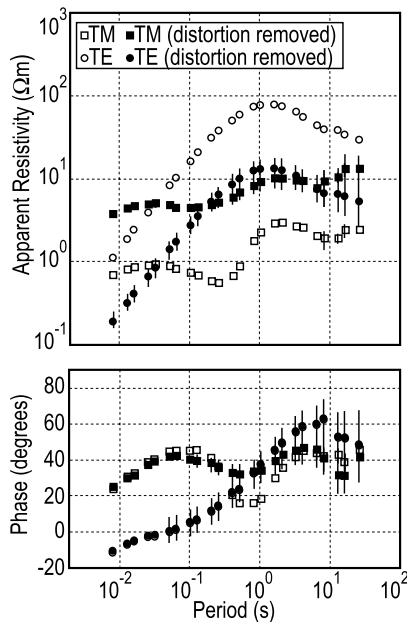


Figure 4. Responses from station 2160E after normal processing (open circles) and after phase tensor distortion removal (closed circles). Distortion removal has shifted the apparent resistivity responses but has made little difference to the phase responses. The negative TE mode phases have not been affected by distortion removal.

phase is also negative, as demonstrated for station 2160E in Fig. 5. Although the phase tensor invariant phases are free from galvanic effects (Caldwell *et al.* 2004) these anomalously low phases must, by definition, be inductive.

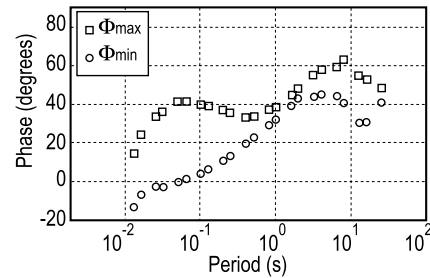


Figure 5. Phase tensor invariant maximum phase (Φ_{\max} , squares) and minimum phase (Φ_{\min} , circles) for station 2160E. Φ_{\min} has negative values at periods that correspond to negative TE mode phases. Because the phase tensor is independent of galvanic distortion, the negative Φ_{\min} values cannot be caused by galvanic distortion and must be an inductive effect.

4 NUMERICAL MODELLING OF 2-D TE DISTORTIONS

4.1 Characterizing the cause of distortions

The survey region appears to approximate the model of Parker (2010) that produces negative TE phases at short periods, with the sedimentary cover acting as the shallow, low resistivity region and the basement acting as the high resistivity region that sits beneath and adjacent to it. To test whether inductive effects in the survey region can create negative phases in the TE mode, forward models were run with the code of Wannamaker *et al.* (1987). The forward models were a simplification of the survey region, consisting of a shallow conductor of thickness (h) 10, 20 and 50 m that extends over one half of the model space with a vertical boundary at the centre of the model (Fig. 6). Responses were calculated with the

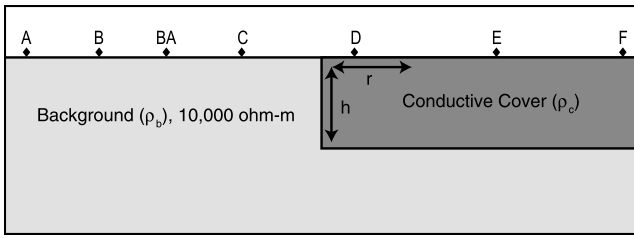


Figure 6. Forward model parameterization where ρ_c is the resistivity of the conductive cover, h is the thickness of the conductive cover and r is the distance from the bounding edge of the cover. For the Occam forward model, synthetic stations were placed at the same intervals as survey stations along the 2160 line for comparison with model responses.

resistivity of the conductor (ρ_c) set to 1, 10 and 100 Ωm and the rest of the model space set to a uniform resistivity of 10 000 Ωm . The model space extends approximately 73 km laterally on each side of the stations and to a depth of approximately 162 km. Stations were set at the same spacing as those along the survey profile 2160 to allow direct comparison of station and forward responses but the responses were calculated at a greater bandwidth than exists for the real data (periods of 0.0001–100 s) to enable analysis of the behaviour at shorter periods than those collected.

Forward model apparent resistivity and phase responses for a station on the resistor (station B) and a station on the conductor (station D), for all calculated thicknesses and resistivities of the conductor, are shown in Fig. 7. At station D, the underlying conductive layer results in very small phases at the shortest periods, which for several of the models extend to small negative phases. The model consisting of a 1 Ωm conductor with thickness 10 m (solid black line) produced negative TE mode phases at periods of 0.002–0.007 s,

while a conductor of the same resistivity but thickness 20 m (solid mid-grey line) produced negative phases at slightly longer periods of 0.007–0.01 s. The model consisting of a 10- Ωm conductor with thickness 10 m (dashed black line) produced a negative TE mode phase at station D at a period of 0.0004 s. Therefore, a simplified 2-D version of the survey region in which a shallow, low resistivity zone with a nearby bounding edge sits on a high-resistivity zone will create negative TE phases at certain periods given appropriate depths and resistivity contrasts.

To extend this analysis to a general case and investigate the physical cause of the negative phases, a Poynting vector analysis (Stratton 1941) was performed. Poynting vectors are a construct for showing the time-averaged energy flux and diffusion path of the EM field; they have recently become a common place tool for studying diffusion in the marine controlled-source EM method (e.g. Weidelt 2007; Chave 2009). The time averaged Poynting vector \vec{S} can be computed from the electric and magnetic fields using

$$\vec{S} = \frac{1}{2} \Re (\vec{E} \times \vec{H}^*), \quad (1)$$

where $*$ denotes the complex conjugate. Although the magnitude of \vec{S} shows the time averaged energy flux, the direction of the Poynting vector can be interpreted as the predominant path of EM diffusion. Plots of the Poynting vectors throughout a 2-D model were used by Key & Constable (2011) to generate new insights on negative phases observed in seafloor MT data. For this study, we used the same 2-D model as above but computed the TE electric field and MT responses throughout the entire model domain using a parallel adaptive finite element code (Key & Oval 2011).

Fig. 8 shows streamlines of \vec{S} at periods of 0.01 s and 1 s for a 5 m thick 1 Ωm layer extending from the origin to the right of the model space. At 0.01 s period, the energy diffuses vertically down into the Earth both on the resistive side of the model space and at a distance

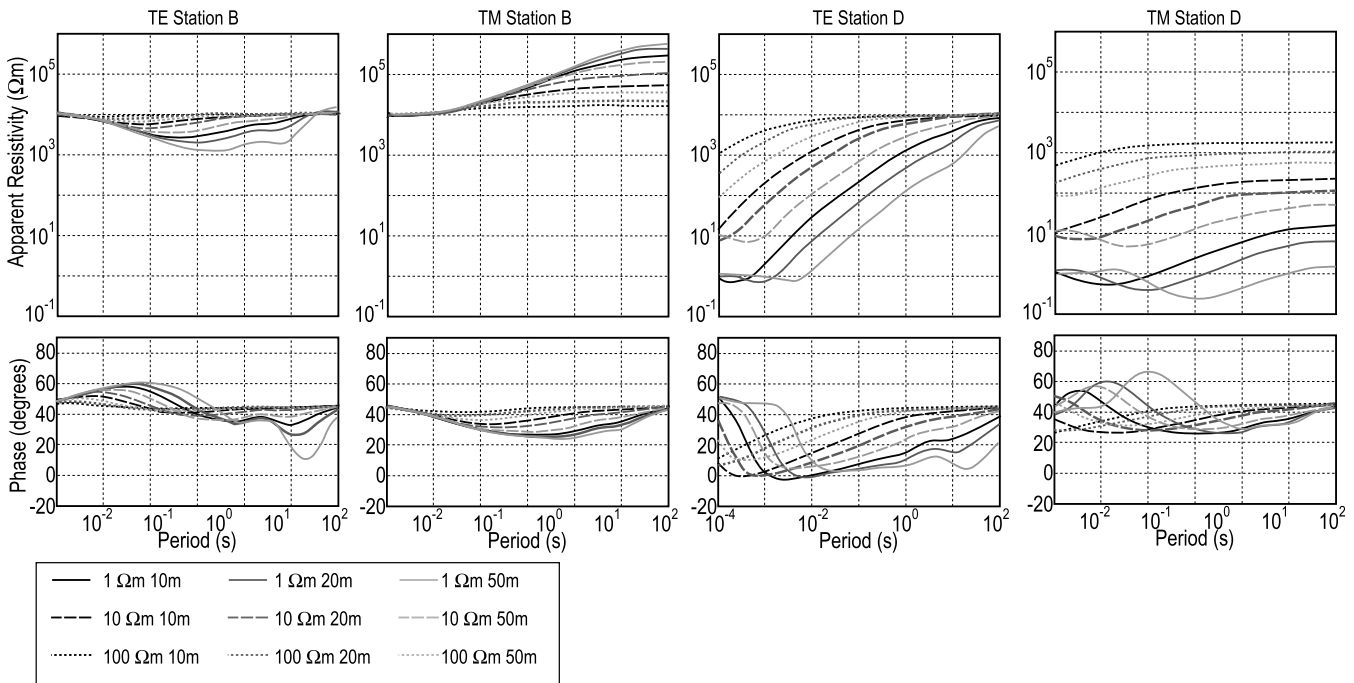


Figure 7. Responses from forward models consisting of a resistive half space of 10000 Ωm that is covered in its northern half by a shallow, low resistivity layer of resistivities 1 Ωm (solid lines), 10 Ωm (dashed lines) and 100 Ωm (dotted lines) and thicknesses 10 m (black lines), 20 m (medium grey lines) and 50 m (pale grey lines). Station locations were set to be equivalent to those for the 2160 line of the station data (Fig. 1) and responses are shown for station B that sits on the resistor and station D that sits on the shallow, low resistivity layer. Forward models in which the low resistivity layer is 1 Ωm and 10 m thickness, 1 Ωm and 20 m thickness and 10 Ωm and 10 m thickness all produce negative phases in the TE mode for stations sitting on the low resistivity layer.

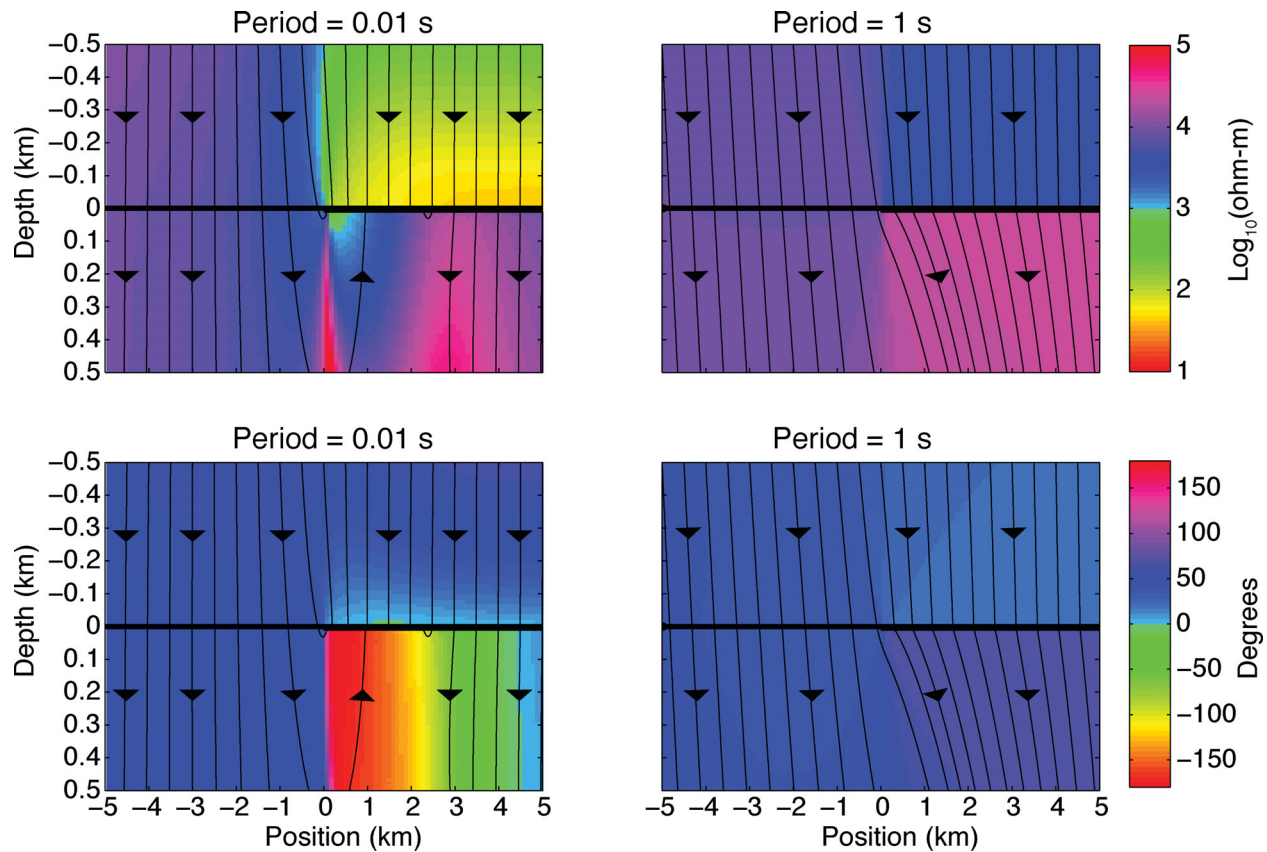


Figure 8. Streamlines of TE Poynting vectors (thin black lines) at periods of 0.01 and 1.0 s for a subsurface of resistivity $10\,000\ \Omega\text{m}$ with a 5 m thick, $1\ \Omega\text{m}$ low resistivity zone extending from the origin to beyond the right side of the figure. Colour contours in the top figures are the TE apparent resistivity and in the bottom figures are TE phase. At 0.01 s, between 0 and 3 km, the TE field energy diffuses upwards towards the surface due to inductive coupling between the high and low resistivity layers.

greater than 3 km from the edge of the conductor on the conductive side of the model space. This predominantly vertical diffusion is expected for typical MT induction. However, at a position of 0–3 km the streamlines curve upwards at depth and diffuse back up to the Earth's surface due to inductive coupling between the resistive basement and the low resistivity cover. In comparison, the streamlines at a 1 s period do not show this extreme inductive coupling and instead diffuse into the Earth in a predominantly downward manner that is typical of MT induction. Colour contours on the top row of Fig. 8 show the TE apparent resistivity across the model space. At 0.01 s, the apparent resistivity beneath the surface is decreased by approximately an order of magnitude at the locations where the streamlines trend upwards. This shows that the upward diffusing energy is sensitive to the conductor above, much in the same way that normal downward diffusing MT energy is sensitive to conductors beneath. Colour contours on the bottom row of Fig. 8 show the TE phase, which exhibits extreme excursions associated with the zone where the energy diffuses upwards toward the Earth's surface at 0.01 s period, while there is no anomalous phase behaviour at 1 s period where the energy is diffusing downwards. At 0.01 s, the largest excursions in phase occur beneath the low resistivity layer and close to its bounding edge, where phase wraps through a full 360° variation. Although the variations are less pronounced, the anomalous phase values, including a zone of small negative phases, extends past the top of the low resistivity layer into the air.

The Poynting vector analysis shows that TE data in the modelled system behave in an analogous way to the TE data on the ocean

side of the coast effect (Key & Constable 2011). The difference between land and marine data is the location of the MT receiver, which sits on the surface of the low resistivity zone on land and at the base of it for a marine survey. Fig. 9 shows streamlines of the Poynting vectors at 0.01 s period (as described above) but now focused on the area immediately surrounding the bounding edge and the base of the low resistivity layer (note the extreme vertical exaggeration). For this image we computed the MT responses and TE field components at 23111 receivers positioned on a grid spaced every 0.1 m vertically and every 50 m horizontally. The colour contours on the upper figure show the Poynting vector magnitude; those on the middle panel show the TE apparent resistivity and those on the lower figure show TE phase. The Poynting vector streamlines reveal the presence of a 'collision zone' close to the base of the low resistivity layer where downward diffusing energy collides with upward diffusing energy, resulting in the vectors being deflected to the right, away from the edge of the low resistivity layer. In the collision zone, there is a peak (or cusp) in the apparent resistivity, as is observed in the ocean side of the coast effect of marine MT data (Constable *et al.* 2009; Key & Constable 2011). The phase abruptly transitions from having moderately negative values above the collision zone to large negative values below it. At the land surface, this behaviour has been smoothed by the low resistivity layer but the region of negative phases extends to the surface and into the air between the 0.5 and 4 km lateral position. Therefore, the physical cause for the negative TE phases observed and modelled for a land survey, in which the recorders sit on top of a

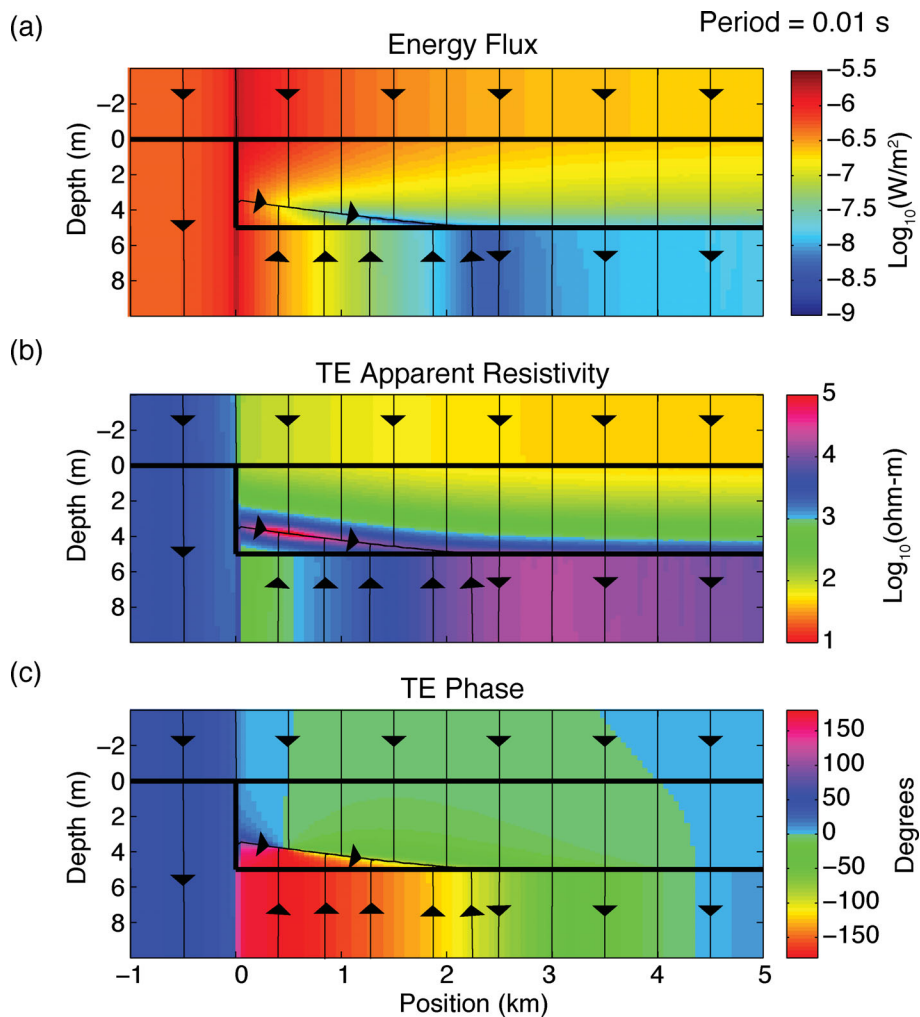


Figure 9. An enlargement of the TE Poynting vector streamlines (thin black lines) shown in Fig. 8 around the boundary of the low resistivity layer (thick black lines) for 0.01 s period, with extreme vertical exaggeration of approximately $\times 430$. Colour contours show the Poynting vector energy flux (a), the TE apparent resistivity (b) and the TE phase (c). Inductive coupling causes the Poynting vectors to diffuse to the right near the boundary of the low resistivity layer, where upward and downward diffusing energy collides, resulting in a subhorizontal band of low energy flux near 3–5 m depth inside the left portion of the conductive layer. In this collision zone the apparent resistivity cusps to exceedingly large values while the phase wraps through 180° . Large negative phases are seen at depths below the collision zone where the energy flux is upwards. Smaller negative phases continue above the collision zone and into the air. To the left of the conductor and to the right at positions exceeding 4 km, the phases are positive as expected for normal undistorted TE responses. The response data were computed on a grid spaced 0.1 m vertically and 50 m horizontally.

low resistivity layer bounded by a high resistivity layer, is the same as that for a marine survey in which the recorders sit on the base of low resistivity sea water bounded by high resistivity seafloor. This cause is the upward diffusion of TE energy caused by inductive coupling between the low and high resistivity zones. Apart from physical scaling, the difference between these systems is only the placement of the MT receivers which has the result that the effects are more extreme in the marine case, as observed by larger negative phases, phase wrapping and apparent resistivity peaks. However, the negative phases can extend to the surface and will be observed in land surveys.

In the appendix we present some basic theory on the MT response behaviour resulting from the superposition of downward and upward travelling plane-waves in a half space. When the energy is dominated by downward diffusion, the MT phase takes on its nominal phase of 45° . Conversely, when the energy is dominated by upward diffusion, the MT phase will be -135° . When both the upward and downward energy are of similar magnitude, the MT response behaviour is more

complicated; in the case of equal magnitudes for the upward and downward travelling energy, the MT response will become singular due to a cancellation of the horizontal magnetic field, leading the observed cusps in apparent resistivity. This cancellation effect is supported by the significantly lower energy flux in the collision zone, as shown in the top panel of Fig. 9. It is the presence of a small yet significant component of upward travelling energy that leads to the small negative phases on land and in the air, as shown in the bottom panel of Fig. 9.

4.2 Characterizing the range of conditions that produce negative phases

The forward model studies provide evidence that the resistivity contrast between the low and high resistivity units and the thickness of the low resistivity unit determine whether negative TE phases are observed and, if they are, at what periods and distance from the boundary they are observed. To explore this more fully, a general

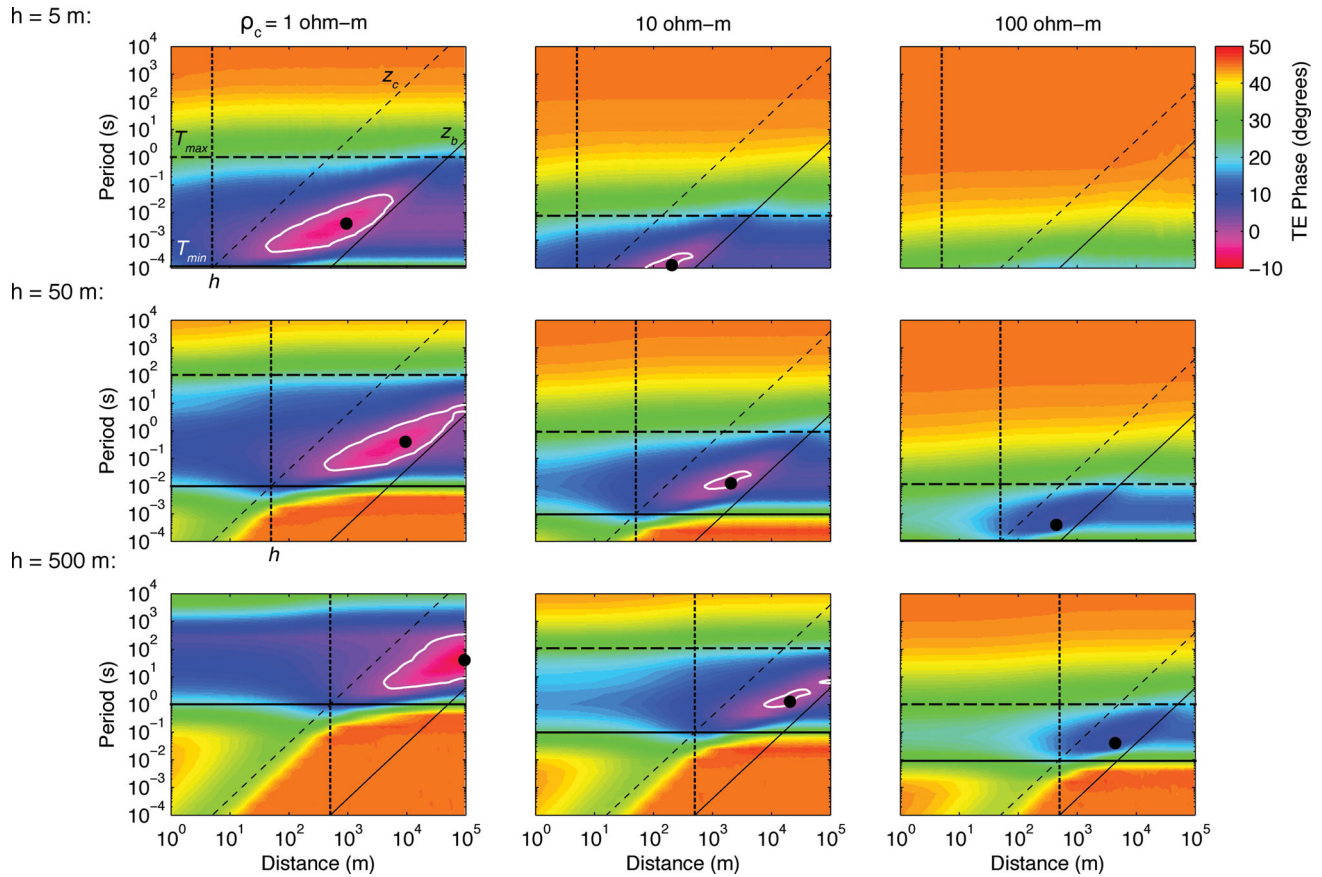


Figure 10. The TE phase shown as a function of period and distance from the boundary of the low resistivity layer (r) for resistivities (ρ_c) of 1, 10 and 100 Ωm and thicknesses (h) of 5, 50 and 500 Ωm . Background resistivity is 10 000 Ωm . Diagonal lines show the skin depths for the low resistivity layer (z_c) and the high resistivity layer (z_b). Horizontal lines show T_{\min} and T_{\max} from eqs (3) and (4). Vertical dashed lines show the thickness of the low resistivity layer. White contours outline the region of negative phases. Black dots show the range and period of the negative phase minimum predicted by eqs (5) and (6).

model was set up consisting of a low-resistivity layer overlying a high-resistivity layer with a bounding edge, as described above (Fig. 6). The high resistivity region was set to 10 000 Ωm while the low resistivity region (ρ_c) varied between 1 and 100 Ωm and the thickness of the low resistivity region (h) varied between 5 and 500 m. Fig. 10 shows the TE phase as a function of period and distance from the boundary for the low resistivity values of 1, 10 and 100 Ωm (columns) and thicknesses (h) of 5, 50 and 500 m (rows).

Negative phases are only observed when $\rho_c \leq 10 \Omega\text{m}$, suggesting that a resistivity contrast of greater than 1000 between the high- and low-resistivity regions is required before negative phases will be observed. Although not shown, we also tested $\rho_c = 20 \Omega\text{m}$ and no negative phases were observed; similarly, a model with $\rho_b = 1000 \Omega\text{m}$ did not produce negative phases until $\rho_c \leq 1 \Omega\text{m}$, again reinforcing that the resistivity contrast appears to be a crucial factor in generating the negative phases.

Fig. 10 shows that all negative phases lie at distances from the lateral 2-D contact that are between the skin depth z_c of the low resistivity unit and the skin depth z_b of the high resistivity unit, where the skin depth z is given by

$$z = \sqrt{\frac{\rho T}{\pi \mu}} \approx 500 \sqrt{\rho T} \text{ m}, \quad (2)$$

where T is the period in seconds. This is somewhat curious since one might expect that the effect of the 2-D edge would be negligible

at distances that are electromagnetically far away when measured in terms of the conductive layer's skin depth, particularly since for land MT the measurement is made on top of the conductive layer. For example, consider the 5 m thick, 1 Ωm model (upper left corner in Fig. 10). At 1 km from the lateral edge, negative phases are observed around 0.001–0.01 s. This corresponds to skin depths of 15–50 m in the low resistivity layer. In other words, the negative phases at 1 km distance are located 20 to 70 skin depths away from the lateral contact. However, the key concepts to note are that the 5 m thick layer is less than one skin depth thick and the skin depths in the resistive basement at these periods are 5–15 km, several times greater than the distance to the contact. Taking these findings along with the Poynting vector analysis, we conclude that the negative phases are generated by anomalous lateral diffusion around the base of the conducting layer. This laterally diffusing energy then travels back up through the thin conductive overburden to produce the negative phase. This distortion is bound at large distances from the lateral edge by the diminishing amplitude of the laterally diffusing energy, which by one resistor skin-length distance from the lateral edge becomes too low amplitude to overwhelm the 'normal' energy that is diffusing down from above.

The skin-length arguments provide bounds on the distances at which the negative phase region can occur at a given period; now we will examine bounds for the period range of the negative phase region. There is a simple geometric dependence on the thickness of the low resistivity layer. Fig. 10 shows that for a given resistivity contrast, the period range of the negative TE phase region

changes in proportion to the square of the thickness. For a given thickness, an increase in resistivity results in the negative phase region moving to shorter periods; additionally, the negative phase region extends across a significantly smaller period and distance range. From Fig. 10 we see that the negative phases always appear at periods where the conductor skin depth is greater than the layer thickness. Thus, the minimum period T_{\min} of the negative phase region follows the inequality

$$T_{\min} > \frac{h^2 \pi \mu}{\rho_c} \quad (3)$$

By inspection, we also find that the maximum period of the anomalous region T_{\max} follows the inequality

$$T_{\max} < \frac{\rho_b T_{\min}}{\rho_c} = \frac{\rho_b h^2}{\rho_c^2} \pi \mu. \quad (4)$$

Fig. 10 shows that the parallelogram formed from these period and the skin depth bounds completely encloses the negative phase region for each model.

For the analysis of the marine TE distortion, Key & Constable (2011) found that the period and range dependence of the apparent resistivity distortion could be fit by empirically derived equations. Here, we have found similar characteristic equations that describe the location of the minimum phase (most negative value) for the land based TE distortion

$$T = \frac{a \rho_b h^2}{\rho_c^{\frac{2}{3}}}, \quad (5)$$

$$r = \frac{b \rho_b h}{\rho_c^{\frac{2}{3}}}, \quad (6)$$

where the constants $a = 1.6 \times 10^{-8}$ and $b = 0.019$. We found these forms by extending our model studies to include $\rho_c = 1, 2, 3, 5, 10 \Omega\text{m}$ and then inspecting the period and range dependence of the minimum phase produced by each model, which yielded the exponents for ρ_c and h . The coefficients a and b were then found by least-squares fits of the above equations to the period and ranges of the minimum phases from the model studies. Black circles in Fig. 10 show the period and range that fulfil these equations for the modelled systems, illustrating that they produce a reasonable fit to the location of the most negative phase. We note that the coefficients a and b and the terms in the denominator are different from those found in Key & Constable (2011), with the likely explanation being that here we are considering the MT distortion that arises on the top of the conductive layer, rather than on the bottom (i.e. the seabed in their study).

Another notable geometric aspect of the distortion is that it tends to appear at distances where r/h is significantly greater than 10 (and more typically at least 100). This may explain why such a simple explanation for negative TE phases has eluded discovery until recently. It may be that such thin elongate layers are rare and furthermore are not often found with underlying resistive layers of high enough contrast (>1000) to generate the lateral TE distortion.

5 INVERSION OF DISTORTED DATA

Because the described TE mode negative phases are an inductive phenomenon and can be produced through forward modelling, it is reasonable to assume that inverse modelling of data containing negative TE phases should reproduce an accurate subsurface structure.

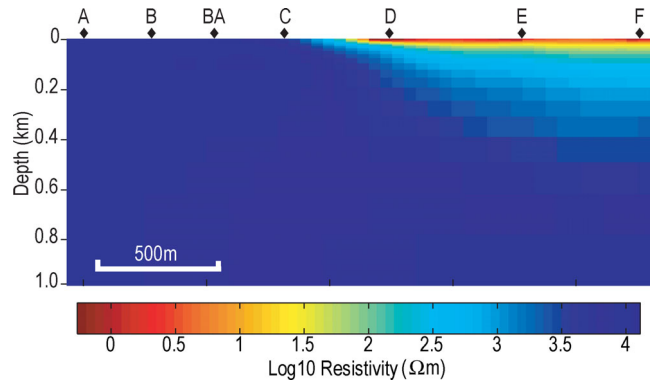


Figure 11. 2-D Occam inversion of synthetic data produced from the 1 Ωm , 10 m thick low resistivity layer model (Fig. 6) has reproduced the subsurface structures and the negative phases.

To test this, synthetic data produced by the forward model consisting of a 10 m thick, 1 Ωm low resistivity zone over a 10 000 Ωm high resistivity zone (Figs 6 and 7) were inverted using the finite element based inversion code Occam2DMT (deGroot-Hedlin & Constable 1990). The model was parameterized into 1029 parameters and a total of 700 apparent resistivity and phase data were inverted from periods of 0.0001–100 s. The model space was the same as the forward models and extended to approximately 73 km laterally on each side of the stations and to a depth of approximately 162 km. Gaussian random noise of 5 per cent were added to the synthetic apparent resistivity and phase data. After 20 iterations, the inversion obtained an rms misfit of 1; all data were closely fit, including the negative TE phases. The inverse model is shown in Fig. 11 to a depth of 1 km. The 10 m thick, 1 Ωm low resistivity zone has been reproduced with considerable accuracy, although sharp edges have been smoothed as is expected for a roughness-stabilized MT inversion (deGroot-Hedlin & Constable 1990).

The accurate reproduction of the synthetic model by inversion of the synthetic data allows confidence that an inversion of the central Australian MT data will accurately reproduce subsurface features. Therefore inverse models of station data along the 2160 line (Fig. 1) were produced using the Occam2DMT code (deGroot-Hedlin & Constable 1990) along a profile oriented north–south with error floors of 5 per cent applied to the data, using the same model space as that described above. Separate models were run of TE-only, TM-only and joint TE and TM data. Only data from periods less than or equal to 1 s were inverted since shallow features were of interest and the phase tensor data suggest that more regional features may begin to affect the data at longer periods. Inverse models are shown to a depth of 600 m in Fig. 12 and data fits for stations 2160B and 2160E are shown in Fig. 13. The inverse models of joint TE and TM mode data (Fig. 12a) and of TE-only data (Fig. 12b) show very similar features. The bulk of the subsurface in these models has an approximately uniform resistivity of $\sim 1000 \Omega\text{m}$ for the joint model and $\sim 10000 \Omega\text{m}$ for the TE model. Both models show a shallow, highly conductive zone at the surface that extends partly under station 2160C but dominantly exists in a single layer beneath stations 2160D, 2160E and 2160F. In both models this layer has a resistivity of $\sim 1 \Omega\text{m}$ and a thickness of $\sim 10\text{m}$. This bears a remarkable similarity to the results of the forward modelling, which showed that a low resistivity zone with these characteristics will produce negative phases in the TE mode at the periods observed in the station data. The other feature evident in these models is a

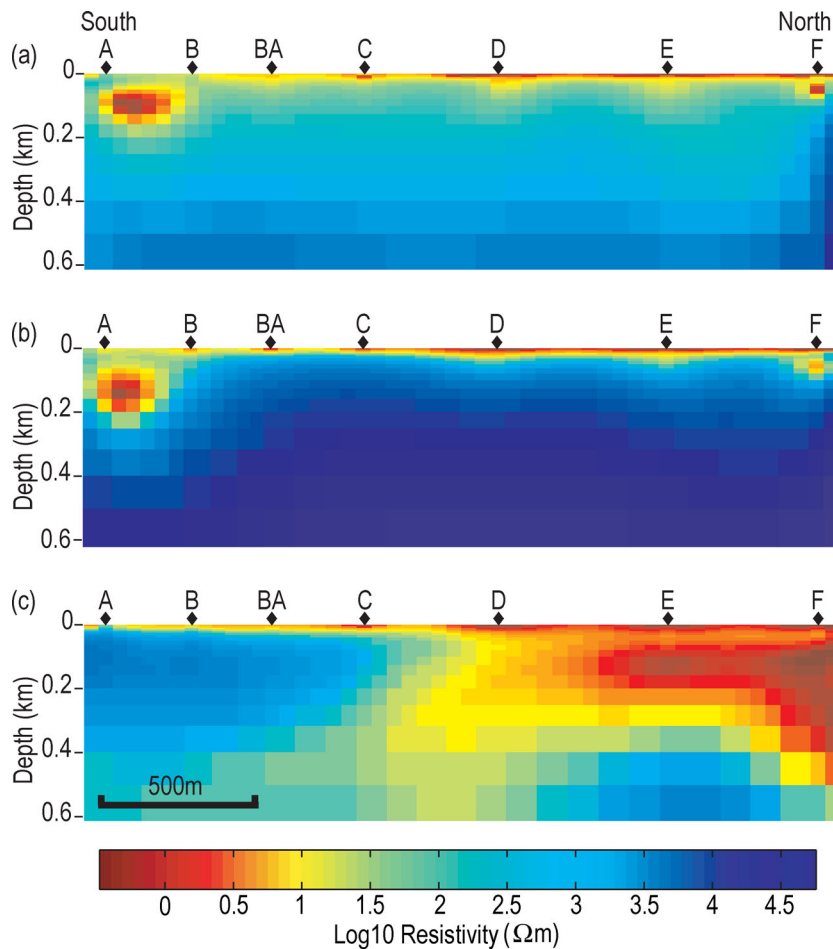


Figure 12. 2-D Occam inversions of data along the 2160 line. Model (a) is an inversion of both TE and TM mode data and inverted to an rms error of 5.45. Model (b) is an inversion of TE data and inverted to an rms error of 5.94. Model (c) is an inversion of TM mode data and inverted to an rms error of 1.3. All models image a low resistivity zone in the northern half of the survey area and the models that incorporate the TE mode have imaged a zone of approximately 1 Ωm and 5–10m thickness.

low resistivity zone at a depth of approximately 30–100 m between stations 2160A and 2160B. The existence of this zone could be a reason why the data from stations in the southern end of the survey show more complexity than those predicted by the forward models. Both the joint TE and TM model and the TE-only model have high rms error values. For the joint model, the rms error is 5.45 and the misfit is mainly contained in the TM mode phase and in offsets in apparent resistivity that appear to be caused by static shifts (Fig. 13, solid lines). For the TE-only model, the rms error is 5.94 and the misfit is mainly contained in the phase of stations in the southern half of the model and in apparent resistivity static shifts (Fig. 13, black dashed line). Importantly, the models accurately reproduce the negative TE mode phases for all stations in which they are observed (Fig. 13). Therefore, despite the large rms errors that may draw into question some features of the models, we are confident that the shallow, low resistivity zone in the northern half of the inversions is a robust product of the negative TE mode phases. The TM-only inverse model (Fig. 12c) contains a low resistivity zone that extends from approximately 30–500 m depth in the north of the model. However, the very shallow (10 m depth), very low resistivity zone ($\sim 1 \Omega\text{m}$) observed in the joint TE and TM and the TE-only models is also apparent in the TM-only model as a separate feature to the slightly deeper, low resistivity zone. The

TM-only model has inverted to an rms error of 1.3 and data fits are very good at all stations (Fig. 13, grey dotted line).

6 DISCUSSION

In contrast to models that explain anomalous phases through complex, 3-D geometries (Egbert 1990; Heise & Pous 2003; Weckmann *et al.* 2003a,b; Ichihara & Mogi 2009; Thiel *et al.* 2009) we have demonstrated that a very simple, 2-D system can produce negative TE mode phases on land as well as in a marine setting. Indeed, the system is so simple that it is perhaps surprising that negative TE phases are not observed more often. Analysis of synthetic data (Fig. 10) has shown that a resistivity contrast greater than 1000 is necessary to produce negative phases and such a contrast is not unreasonable between resistive basement and sedimentary cover. However, the analysis also showed that while negative phases will be seen at locations close to the boundary of thin, low resistivity layers, thicker conductive layers must have a significant lateral extent in order for negative phases to be observed (Fig. 10). For instance, a 5 km thick, 1 Ωm layer in a 10 000 Ωm half-space produces negative phases that do not appear until periods somewhere in the range of 100–1 000 000 s and at distances greater than 100–1000 km from the edge of the low resistivity layer (from eqs 3–6); such

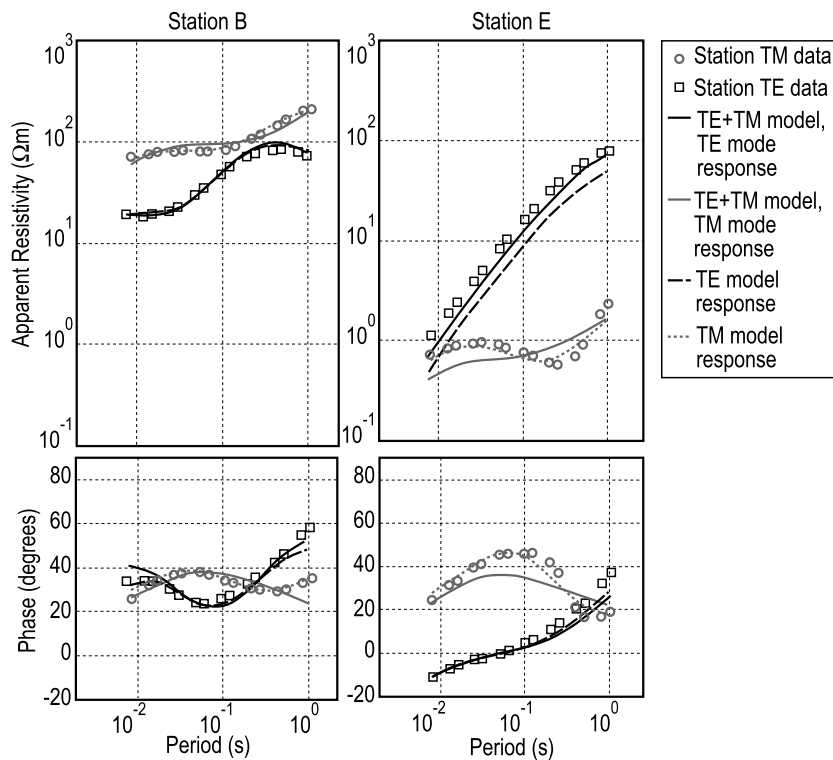


Figure 13. Data fits for representative stations B and E. Station data for the TE mode are shown as black squares and the TM mode as grey circles. Model responses from the joint TE and TM mode model are shown as solid lines, from the TE mode model as dashed lines and the TM mode model as dotted lines for the TE mode in black and the TM mode in grey.

a large lateral extent for a 2-D layer is physically unlikely given the complexity of near surface geology. In addition, the system requires the existence of an outcropping boundary between the low and high resistivity regions, whereas many thin, laterally continuous, conductive layers may have geometrically complex boundaries or may be bound by other conductive bodies.

The survey region in central Australia satisfies the requirements for producing negative phases, with a bounded, thin, laterally continuous conductor. Sedimentary cover in Australia is generally imaged to have very low resistivity, often significantly less than $10 \Omega\text{m}$ (e.g. Asten 1992; Macnae *et al.* 2001; Mudge 2004) due to the high volumes of salt in sediment and groundwater (Rengasamy 2006). The months preceding the data collection in central Australia saw some rainfall in the region and additional rain also fell during the field work, which may have increased the mobility of salts in the sediment and resulted in the very low resistivities of between 1 and $10 \Omega\text{m}$ observed in the forward and inverse modelling.

Although the physical requirements for this system may not be commonly met, they are certainly not unique in being met in this particular location in central Australia. There are well-documented cases where anomalous phases have been shown to be generated by complex 3-D structures, anisotropy or coherent noise. In particular, anomalously large phases for land MT (values greater than 90°) can be explained by these factors while we have found no evidence that they can be accounted for by the 2-D system we have presented. However, we suspect that there are also instances where negative TE phases have been incorrectly assumed to be caused by these factors, but in fact are the result of the simple 2-D TE mode system we have described. It is also curious that the analytical discovery of negative 2-D TE phases for land MT apparently did not occur until

the work of Parker (2010); perhaps the extreme nature of the thin conductive layer and the correspondingly unusual negative phases left earlier investigators to doubt the reliability of their numerical algorithms. Here, we have documented that the negative phases can be robustly predicted by two completely independent finite element codes (Wannamaker *et al.* 1987; Key & Owall 2011) and one analytical method (Parker 2010).

Finally, we note that we also tried reproducing the negative phases for this model using the commercial MT software package WinGLink (software version 2.20.01). However, 2-D forward modelling from the software only produced small positive phases rather than the negative phases generated by the finite element codes. Although this package uses a finite difference method, there is no fundamental reason why a finite difference algorithm should not be able to produce negative TE phases. However, since the source code for this ‘black box’ package is unavailable, we are unable to further investigate the cause of the disagreement.

7 CONCLUSIONS

Negative phases in the TE mode of land-based magnetotelluric data have historically been attributed to coherent noise or complex 3-D geometries. However, we have shown that a shallow, laterally extensive, bounded, low resistivity zone that overlies a higher resistivity region with sufficient resistivity contrast (1000 or greater) can also produce negative TE mode phases. This is the first time that a simple, purely 2-D scenario has been used to explain negative phases in land MT data. Analysis of Poynting vectors shows that the negative phases are caused by a collision between ‘normal’ TE field energy that is diffusing downwards with energy that has been inductively

coupled between the high and low resistivity layers and is travelling back upwards. This inductive cause of anomalous phases is a correlative of the ocean side of the coast effect observed in marine MT data (Fischer 1979; Constable *et al.* 2009; Key & Constable 2011). The only difference between the two systems is that the effects of the inductive coupling are less extreme when measured on the surface of the conductor in a land survey than on the base of the conductor in a marine survey due to the smoothing effect of the conductor itself. As is the case for marine data, the characteristic frequency range and distance from the boundary of the conductor at which negative TE phases are observed can be estimated from a simple combination of the resistivities of both the low and high resistivity regions and the thickness of the conductor. A grid of broad-band MT data collected in central Australia over an area that transitions from subcropping basement rocks to sedimentary cover at least several metres thick is an example of this physical system. Stations located on the conductive sedimentary cover uniformly exhibit negative phases in the TE mode while stations located on subcropping resistive basement rocks do not have negative phases. The spatial pattern of the observed MT responses demonstrates they are related to the geoelectric structure of the subsurface rather than to coherent noise. 2-D inversions of synthetic and station data reproduce the negative phases by modelling a thin, very low resistivity layer beneath the stations located on the cover, and show that a code that can account for negative TE phases such as Occam2DMT (deGroot-Hedlin & Constable 1990) can accurately recover subsurface structure from such data. In many situations where negative TE mode phases are encountered, equivalent spatial coverage may not exist (e.g. Thiel & Heinson 2010) and it may not be possible to evaluate the possible influence of coherent noise. However, these results provide an alternative, inductive explanation for negative TE mode phases that should be considered when analysing anomalous data.

ACKNOWLEDGMENTS

The authors are very grateful to O. Ritter for his careful editorial handling and to U. Weckmann and two anonymous reviewers for their helpful suggestions that improved the manuscript greatly. S. Constable and students are gratefully acknowledged for their useful suggestions about the coast effect in early discussions. H. Adam assisted with the fieldwork. KS's fellowship during this work and research funding were supplied by ARC project 09ARC_DP0988263. This contribution forms TraX record 197.

REFERENCES

Asten, M.W., 1992. Interpretation of ground TEM data from conductive terranes, *Explor. Geophys.*, **23**, 9–16.
 Bibby, H.M. & Hohmann, G.W., 1993. 3-dimensional interpretation of multiple-source bipole-dipole resistivity data using the apparent resistivity tensor, *Geophys. Prospect.*, **41**, 697–723.
 Bibby, H.M., Caldwell, T.G. & Brown, C., 2005. Determinable and non-determinable parameters of galvanic distortion in magnetotellurics, *Geophys. J. Int.*, **163**, 915–930.
 Caldwell, T.G., Bibby, H.M. & Brown, C., 2004. The magnetotelluric phase tensor, *Geophys. J. Int.*, **158**, 457–469.
 Camacho, A., Vernon, R.H. & Fitz Gerald, J.D., 1995. Large volumes of anhydrous pseudotachylite in the Woodroffe Thrust, eastern Musgrave Ranges, Australia. *J. Struct. Geol.*, **17**, 371–383.
 Chave, A.D., 2009. On the electromagnetic fields produced by marine frequency domain controlled sources, *Geophys. J. Int.*, **179**, 1429–1457.
 Chave, A.D. & Thomson, D.J., 2004. Bounded influence magnetotelluric response function estimation, *Geophys. J. Int.*, **157**, 988–1006.

Constable, S., Key, K. & Lewis, L., 2009. Mapping offshore sedimentary structure using electromagnetic methods and terrain effects in marine magnetotelluric data, *Geophys. J. Int.*, **176**, 431–442.
 Edgoose, C.J., Camacho, A., Wakelin-King, G.A. & Simons, B.A., 1993. *Kulgera 1:250 000 Geological Map Series Explanatory Notes*, Northern Territory Geological Survey.
 Egbert, G.D., 1990. Concerning dispersion relations for the magnetotelluric impedance tensor – comment, *Geophys. J. Int.*, **102**, 1–8.
 Egbert, G.D., 1997. Robust multiple-station magnetotelluric data processing, *Geophys. J. Int.*, **130**, 475–496.
 Egbert, G.D., 2002. Processing and interpretation of electromagnetic induction array data, *Surv. Geophys.*, **23**, 207–249.
 Ferguson, I., 1988. The Tasman Project of Seafloor Magnetotelluric Exploration, *PhD thesis*, Australian National University, Canberra.
 Fischer, G., 1979. Electromagnetic induction effects at an ocean coast, *Proc. IEEE*, **67**, 1050–1060.
 Fischer, G., Schnegg, P.A. & Usadel, K.D., 1978. Electromagnetic response of an ocean-coast model to E-polarization induction, *Geophys. J. R. astr. Soc.*, **53**, 599–616.
 deGroot-Hedlin, C. & Constable, S., 1990. Occam inversion to generate smooth, 2-dimensional models from magnetotelluric data. *Geophysics*, **55**, 1613–1624.
 Heise, W. & Pous, J., 2003. Anomalous phases exceeding 90 degrees in magnetotellurics: anisotropic model studies and a field example, *Geophys. J. Int.*, **155**, 308–318.
 Ichihara, H. & Mogi, T., 2009. A realistic 3-D resistivity model explaining anomalous large magnetotelluric phases: the L-shaped conductor model, *Geophys. J. Int.*, **179**, 14–17.
 Jiracek, G.R., 1990. Near-surface and topographic distortions in electromagnetic induction, *Surv. geophys.*, **11**, 163–203.
 Key, K. & Constable, S., 2011. Coast effect distortion of marine magnetotelluric data: insights from a pilot study offshore northeastern Japan, *Phys. Earth planet. Inter.*, **184**, 194–207.
 Key, K. & Owall, J., 2011. A parallel goal-oriented adaptive finite element method for 2.5D electromagnetic modeling, *Geophys. J. Int.*, **186**, 137–154.
 Lilley, F.E.M. & Weaver, J.T., 2010. Phases greater than 90 degrees in MT data: analysis using dimensionality tools, *J. appl. Geophys.*, **70**, 9–16.
 Macnae, J., Bishop, J. & Munday, T., 2001. Simplified electrical structure models at AEM scales, Lawlers, Western Australia, *Explor. Geophys.*, **32**, 29–35.
 Mudge, S.T., 2004. Radial resistivity/IP surveys using a downhole current electrode, *Explor. Geophys.*, **35**, 188–193.
 Parker, R.L., 2010. Can a 2-DMT frequency response always be interpreted as a 1-D response? *Geophys. J. Int.*, **181**, 269–274.
 Rengasamy, P., 2006. World salinization with emphasis on Australia, *J. Exp. Bot.*, **57**, 1017–1023.
 Schwalenberg, K. & Edwards, R.N., 2004. The effect of seafloor topography on magnetotelluric fields: an analytical formulation confirmed with numerical results, *Geophys. J. Int.*, **159**, 607–621.
 Selway, K., Hand, M., Heinson, G.S. & Payne, J.L., 2009. Magnetotelluric constraints on subduction polarity: reversing reconstruction models for Proterozoic Australia, *Geology*, **37**, 799–802.
 Selway, K., Hand, M., Payne, J.L., Heinson, G.S. & Reid, A., 2011. Magnetotelluric constraints on the tectonic setting of Grenville-aged orogenesis in central Australia, *J. Geol. Soc. Lond.*, **168**, 251–264.
 Stratton, J.A., 1941. *Electromagnetic Theory*, McGraw-Hill, New York, NY.
 Thiel, S. & Heinson, G., 2010. Crustal imaging of a mobile belt using magnetotellurics: an example of the Fowler Domain in South Australia, *J. geophys. Res.*, **115**, doi:10.1029/2009JB006698.
 Thiel, S., Heinson, G., Gray, D.R. & Gregory, R.T., 2009. Ophiolite emplacement in NE Oman: constraints from magnetotelluric sounding, *Geophys. J. Int.*, **176**, 753–766.
 Wade, B.P., Kelsey, D.E., Hand, M. & Barovich, K.M., 2008. The Musgrave Province: stitching north, west and south Australia, *Precamb. Res.*, **166**, 370–386.

- Ward, S.H., & Hohmann, G.W., 1987. Electromagnetic theory for geophysical applications, in *Electromagnetic Methods in Applied Geophysics* vol. 1, ed. Nabighian, M.N., Soc. Exploration Geophysicists, Tulsa, OK.
- Wannamaker, P.E., Stodt, J.A. & Rijo, L., 1987. A stable finite-element solution for two-dimensional magnetotelluric modelling. *Geophys. J. R. astr. Soc.*, **88**, 277–296.
- Weckmann, U., Ritter, O. & Haak, V., 2003a. Images of the magnetotelluric apparent resistivity tensor, *Geophys. J. Int.*, **155**, 456–468.
- Weckmann, U., Ritter, O. & Haak, V., 2003b. A magnetotelluric study of the Damara Belt in Namibia 2. MT phases over 90 degrees reveal the internal structure of the Waterberg Fault/Omaruru Lineament. *Phys. Earth planet. Inter.*, **138**, 91–112.
- Weidelt, P., 1972. The inverse problem of geomagnetic induction, *J. Geophys. – Z. Geophys.*, **38**, 257–289.
- Weidelt, P., 2007. Guided waves in marine CSEM, *Geophys. J. Int.*, **171**, 153–176.
- Weidelt, P. & Kaikkonen, P., 1994. Local 1-D interpretation of magnetotelluric B-polarization impedances, *Geophys. J. Int.*, **117**, 733–748.
- White, A. & Heinson, G., 1994. 2-dimensional electrical-conductivity structure across the southern coastline of Australia. *J. Geomagnet. Geoelectr.*, **46**, 1067–1081.

APPENDIX: THEORETICAL EXPLANATION OF NEGATIVE PHASES AND APPARENT RESISTIVITY CUSPS

If we assume that a strong component of upward diffusing energy can be generated from inductive coupling near the edge of the 2-D conductive layer (e.g. as shown in Figs 8 and 9), then we can draw upon 1-D theory to explain the causes of negative phases and apparent resistivity cusps. From the behaviour shown in Fig. 9, we can locally approximate the TE energy as the superposition of upward and downward travelling plane waves. In a homogeneous conducting halfspace, the downward and upward travelling waves can be represented according to (e.g. Ward & Hohmann 1987):

$$E = E^+ e^{-ikz} + E^- e^{ikz}, \quad (\text{A1})$$

$$H = H^+ e^{-ikz} + H^- e^{ikz}, \quad (\text{A2})$$

where k is the diffusion constant

$$k = \sqrt{-i\omega\mu\sigma}, \quad (\text{A3})$$

ω is the angular frequency, μ is magnetic permeability, σ is conductivity and z is defined using a right handed coordinate system with z positive down. E^+ is the value of the downward travelling wave at $z = 0$ while E^- is the value for the upward travelling wave, and similarly for the magnetic field. From Faraday's law, the plane wave electric and magnetic fields are related by

$$\frac{\partial E_x}{\partial z} = -i\omega\mu H_y. \quad (\text{A4})$$

The magnetotelluric impedance Z evaluated at $z = 0$ is then

$$Z = \frac{E_x}{H_y} = \frac{\omega\mu}{k} \left(\frac{E^+ + E^-}{E^+ - E^-} \right) = \sqrt{\frac{\omega\mu}{\sigma}} e^{i\frac{\pi}{4}} \left(\frac{E^+ + E^-}{E^+ - E^-} \right). \quad (\text{A5})$$

When there is only the downward travelling wave E^+ , the impedance is

$$Z^+ = \sqrt{\frac{\omega\mu}{\sigma}} e^{i\frac{\pi}{4}}, \quad (\text{A6})$$

where the impedance phase is 45° . Conversely, when there is only the upward travelling wave E^- , the impedance is

$$Z^- = \sqrt{\frac{\omega\mu}{\sigma}} e^{-i\frac{3\pi}{4}}. \quad (\text{A7})$$

where the phase is -135° . When there is a mixture of upward and downward waves, the phase can essentially take on any value because both E^+ and E^- can have arbitrary complex values and the ratio in eq (A5) will take on a complex value. Thus we can see that observations of negative phases can be associated with the dominance of the upward diffusing term. This is in contrast to the usual 1-D MT case where any upward travelling energy is generated from reflections from layers below and is always weaker than the downward travelling energy. The peak in apparent resistivity observed in the collision zone can be explained by noting that this ratio is singular when $E^+ = E^-$. In other words, when the upward and downward travelling waves are of similar size, the fields cancel in the denominator (meaning the horizontal magnetic field collapses), leading to cusps in apparent resistivity at the frequency and position where $E^+ = E^-$.